Molecular Vision 2002; 8:102-13 <http://www.molvis.org/molvis/v8/a14>
Received 29 September 2000 | Accepted 18 February 2002 | Published 8 April 2002

Hammerhead ribozymes designed to cleave all human rod opsin mRNAs which cause autosomal dominant retinitis pigmentosa

Jack M. Sullivan, Kathleen M. Pietras, Bryant J. Shin, John N. Misasi

(The first three authors contributed equally to this publication)

Department of Ophthalmology, SUNY Upstate Medical University, Syracuse, NY

Purpose: Knockdown hammerhead ribozymes were designed to cleave at a sterically accessible site in long expression-competent mutant and normal human rod opsin mRNAs. Ribozyme suppression of mutant mRNA is expected to rescue autosomal dominant retinitis pigmentosa (adRP) caused by rod opsin mutations.
Methods: Energy minimization algorithms predicted regions in human rod opsin mRNA accessible to ribozyme cleavage. Opsin and ribozyme RNAs were generated by in vitro transcription. Ribozyme cleavage reactions were performed in vitro at various enzyme:substrate ratios with appropriate controls and analyzed on denaturing polyacrylamide gels.
Results: A GUC triplet in a predicted unhybridized loop was selected as the target cleavage site. Ribozymes were designed to stabilize catalytic core folding. Ribozyme reactions with normal and representative mutant (C187Y) opsin mRNAs demonstrated a decrease of long and short RNA targets and proportional appearance of cleavage products. Site-specific targeting was proved by lack of cleavage of a normal mRNA engineered with a silently altered cleavage motif.
Conclusions: Knockdown ribozymes, targeting all known adRP mutants, cleaved human rod opsin mRNAs at the intended target site in vitro. These ribozymes may reduce total opsin mRNA and protein in rod photoreceptors as a gene therapy strategy. A beneficial outcome on rod survival in adRP is expected although normal rhodopsin levels, already in excess, would also decrease. Knockdown ribozymes attack an accessible site common to all mutant mRNAs to avoid redesign and optimization for each new dominant mutation. This strategy can be extended to any dominant disease affecting genes normally expressed in excess.

Hammerhead ribozymes (hRz) and other catalytic RNAs are site-specific enzymes with antisense (AS) flanks that hybridize to the target mRNA around the cleavage site [1]. Ideally, the AS flanks bind just long enough to allow the catalytic core of the ribozyme (Rz) to cleave (maximum about 1/min) [2,3]. The two cleavage products may be released allowing the Rz to turnover new targets. Cleaved mRNA is rapidly degraded because the products lose protective effects of 5'-capping or 3' polyadenylation. The number of protein molecules produced from each mRNA is large so even low levels of mRNA knockdown can significantly suppress toxic mutant protein levels. In an elegant proof-of-principle study mutation-specific Rzs (MSpe-Rz) designed to selectively cleave mutant opsin mRNA [4] were effective at slowing retinal degeneration in a transgenic rat model, even though reduction of mutant opsin mRNA was only 10-15% [5]. MSpe-Rz designs require that the mutation generate a new hRz cleavage site (NUH‘, where N=G,A,C,U; H=C,A,U [6,7] and ‘ indicates the site of phosphodiester bond cleavage) that is not present in wild type (WT) mRNA (e.g., GAC->GUC‘: Asp->Val) [8]. The MSpe-Rz approach has therapeutic potential for only 14 of the many known opsin autosomal dominant retinitis pigmentosa (adRP) mutations. A mutation-selective approach (MSel-Rz) covers a wider range of mutations but also leads to cleavage of WT mRNA [4,9].

Nearly a hundred single nucleotide (nt) rod opsin gene missense mutations cause the retinal degeneration autosomal dominant retinitis pigmentosa (adRP) [10]. Different mutations cause diverse clinical phenotypes with variable times of onset and rates of progression [10,11]. Our hypothesis is that suppression of daily toxic mutant opsin expression [12-15] in the photoreceptor would protect against apoptotic cell death [16,17] and prolong the onset and rate of degeneration.

Knockdown (KD) hRzs act to suppress both mutant and normal wild type (WT) target mRNAs to the same extent. The rationale that a KD hRz approach could be therapeutic for opsin adRP is based upon the fact that rhodopsin is abundantly expressed in rod photoreceptors. Single cell physiological studies have shown that only 200 rhodopsin activations will saturate human rod photoreceptor transduction machinery, despite the presence of approximately 10^8 molecules in the rod outer segment [18]. This indicates that rhodopsin levels could be substantially reduced with transduction preserved, albeit at lower sensitivity. At least 50% of human rhodopsin is in excess with respect to rod survival. A recessive human rod opsin mutation (E249ter) in the carrier state causes an expected 50% loss of WT rod visual pigment, yet night vision is reported normal and there is no retinal degeneration [19,20]. The only

Correspondence to: Jack M. Sullivan, M.D., Ph.D., Assistant Professor of Ophthalmology, SUNY Upstate Medical University, Institute for Human Performance, Room 4210, 750 East Adams Street, Syracuse, NY, 13210; Phone: (315) 464-6694; FAX: (315) 464-9942; email: Sullivaj@mail.upstate.edu

result of a single dose of E249ter opsin is a slight but clinically insignificant loss of rod sensitivity. The E249ter null human mutation is comparable to the heterozygous rod opsin knockout mouse, which expresses 50% of normal rod rhodopsin protein from one functional WT allele. The opsin$^{+/-}$ mouse has shortened rod outer segments, a slight loss in rod functional sensitivity, and little, if any, rod photoreceptor cell loss [21]. Mammalian rod photoreceptors tolerate reductions in WT rod rhodopsin at least as much as 50% with little, if any, functional consequences. When WT albino rats are raised in cyclic light (400 lux), dark-adapted rod rhodopsin decreases to 25% of normal with reductions in outer segment length, but little cell death [22]. This suggests that reductions of WT rod rhodopsin in adRP rods to as low as 25%, for example by a 50% hRz-induced reduction of total rod opsin (WT + mutant), may be well tolerated, leaving surviving rods with shorter outer segments. The benefit of reducing toxic mutant opsin in an adRP rod photoreceptor is unlikely to be offset by equivalent suppression of WT protein, so long as sufficient WT rhodopsin remains to support outer segment formation.

As a candidate gene therapy for adRP we developed a panel of KD hRzs to reduce the levels of total rod opsin mRNA. We chose a KD approach [23-26] because higher order mRNA structure imposes a severe constraint on any Rz gene therapy strategy [27-38] (Sullivan et al., in preparation). Most mutations are likely buried in secondary and tertiary structures that inhibit rate-limiting annealing of mutation-directed Rzs [39,40]. Only a handful of cleavage sites are likely accessible in any WT or mutant mRNA. We demonstrate here for the first time that hRzs can specifically cleave long expression-competent functional human rod opsin mRNAs in vitro at physiological temperatures to reduce intact transcript levels significantly. These hRzs cleave mRNAs from WT and severe adRP mutant human opsin (C187Y [41]) alleles equally well and are expected to cleave mRNAs from all known mutant opsin adRP genes as none alter the target site. Preliminary results were reported [25].

METHODS

Materials: Oligodeoxynucleotides (ODNs) were synthesized by GenoSys (The Woodlands, TX). In vitro transcription kits (MegaScript, MegaShortScript) were from Ambion (The Woodlands, TX). SYBR Gold was from Molecular Probes (Eugene, OR).

RNA Secondary Structure Analysis: Opsin mRNA and hRzs were subjected to secondary structure analysis by the Genetics Computer Group (GCG Version 9.1; Madison, WI) [42] algorithms RNAFOLD and MFOLD. RNAFOLD identifies the lowest energy structure at 25 °C [43] and MFOLD shows a range of possible conformations at a user specified temperature [44].

Construction of hRz and Opsin Expression Vectors: First generation hRzs had symmetrical antisense (AS) flank sequences surrounding the consensus catalytic domain [45] (Figure 1). hRz cDNAs and a human WT rod opsin cDNA (1.8 kB) [46] were cloned into pSP64pA (Promega, Madison, WI; first generation) or pCDNA3 (InVitrogen, Carlsbad, CA) downstream from the SP6 or T7 promoters, respectively. Runoff transcription of second generation hRzs from XbaI linearized pCDNA3 yields hRz-containing RNAs with 15 and 1 nucleotides (nts) of vector sequence at the 5' and 3' ends, respectively. Runoff transcription from XbaI linearized pCDNA3 vector leads to an opsin cRNA (1838 nt) extending from the proximal twenty-first nt in the 5'-untranslated leader sequence, through the complete coding region, and through a long 3' untranslated sequence; the size of this opsin cRNA includes 72 and 20 nts of vector sequence at the 5' and 3' ends, respectively. This opsin cRNA is a model for the most abundant in vivo transcript (about 1.8 kB) that terminates after the first polyadenylation signal [46]. ODN-directed mutagenesis [47] of WT human rod opsin cDNA generated the V230V silent opsin mutation [48]. This construct silently changes the V230 codon from the hRz cleavable GUC‘ to a noncleavable GUG and allows tests of cleavage site specificity. Truncated (450 bp) WT and V230V cDNA fragments embracing the V230 codon were cloned in the sense direction into pBluescript-II-KS downstream from the T7 promoter. The same WT truncated (450 bp fragment) cDNA was cloned into pBlueScriptII-SK in an antisense orientation relative to the T7 promoter. The expression plasmid for second generation (second generation) hRz, Rz2A, was prepared by ODN-directed mutagenesis [47] of first generation hRz cDNA in pCDNA3 yielding a unique XhoI site in the StemII/loop (Figure 1). Rz2B was generated from plasmid Rz2A by XhoI fill-in, and resulted in an extension of hRz StemII from four bp (Rz2A) to six bp [49] (Figure 1).

In vitro transcription of ribozymes and opsin cDNAs: Opsin and hRz plasmids were downstream linearized with XbaI while truncated opsin target pBlueScript vectors were linearized with HindIII. Templates were phenol-chloroform extracted, and ethanol precipitated. Runoff transcription in vitro was performed using T7 RNA polymerase according to Ambion’s recommendations (opsin templates: MegaScript; hRz templates: MegaShortScript) with 1 µg of linear template and 7.5 mM of each NTP [50]. Following DNase I digestion of template, RNA was phenol-chloroform extracted, ethanol precipitated, resuspended in RNase-free water, and quantified by spectrophotometry (Beckman DU-640). First generation hRz and opsin mRNAs were transcribed from pSP64pA using SP6 RNA polymerase with opsin mRNA internally labeled with α-^{32}P-UTP.

In vitro ribozyme cleavage assays: Varied molar ratios of target opsin mRNA ([Substrate]=[S]) to hRz RNA ([Enzyme]=[E]) were mixed in a total volume of 5-20 µl of 50 mM Tris-HCl (pH 8.0) [51,52]. E and S were preannealed by simultaneous heat denaturation for 5 s at 95 °C and slowly equilibrated to 37 °C to resolve RNA aggregates and promote E:S annealing [52,53]. Cleavage was initiated by $MgCl_2$ addition to a final concentration of 10 mM or 20 mM, plus 1 mM Na_2EDTA, and allowed to proceed at 37 °C or 50 °C. Reactions were quenched on ice with denaturing urea/EDTA buffer (8 M urea, 50 mM Na_2EDTA, 7.5% (v/v) glycerol, and 0.05% (w/v) bromphenol blue). Products were heated (2 min, 95 °C) before loading and electrophoresed on 4% denaturing

polyacrylamide:urea (8.3 M) gels at constant wattage (temperature: 55-60 °C). Gels used to analyze first generation hRz cleavage reactions were dried and autoradiographed (KODAK XOMAT film; Eastman Kodak, Rochester, NY). Gels from second generation hRz cleavage assays were stained for 15 min with SYBR Gold (detection sensitivity about 40 pg/band; 1:10,000 dilution in 1X TBE buffer). Fluorescence was excited at 300 nm and emission photographed through a Wratten 15 filter (longpass > 510 nm) on a gel documentation system (MP-ST, FOTODyne, Hartland, WI).

hRz cleavage reactions were also conducted during in vitro transcription. Linearized E and S plasmids were mixed to define true template molar ratios and transcription (T7-MegaScript) occurred for 1 h at 37 °C. In this paradigm both E and S RNAs are concurrently synthesized to participate in hRz cleavage reactions. Products were either phenol-chloroform extracted and ethanol precipitated prior to mixing with gel loading buffer or quenched after synthesis with ice-cold gel loading buffer, then heat pulsed and electrophoresed as above on 4% polyacrylamide-urea gels. During transcription/cleavage reactions total Mg^{2+} concentration is between 20-30 mM [50] (typically about 30 mM) as optimized by Ambion to maximize RNA yield for each lot of MegaScript.

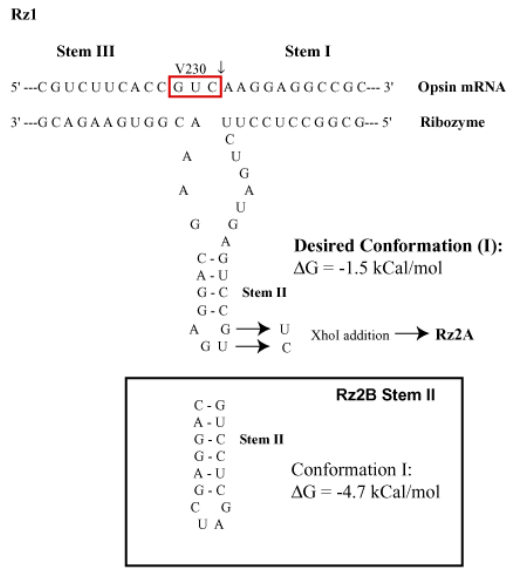

Figure 1. Design of first and second generation anti-V230 KD hRzs. The catalytic consensus core of the hRz is embraced by the AS flanks (5': 11 nt; 3': 12 nt) to create the first generation anti-V230 hRz. The AS flanks base pair with the opsin mRNA to form Stems I and III. The GUC‘ cleavage site is shown (red box). The folding energy of the active conformation (shown) of the first generation hRz is shown. The AS flanks of the first generation hRz were maintained in second generation hRzs (Rz2A and Rz2B). To create Rz2A two nucleotides in the Stem II tetraloop that were predicted to cause first generation hRz misfolding and inactivity were replaced (arrows) to generate a unique XhoI site for the hRz plasmid (pCDNA3). Rz2A has four base pairs in Stem II and the expected conformation was the most stable structure (ΔG=-1.5 kCal/mol) relative to random coil. To create Rz2B the XhoI site was restricted, filled-in and religated to extend Stem II (inset) from four to six base pairs. ΔG of folding of Rz2B is -4.7 kCal/mol or -3.2 kCal/mol more stabile than Rz2A.

HEK293S cell transfection and opsin immunocytochemistry: HEK293S cells [54] grown in 10 cm or 6 well dishes were transfected (calcium phosphate or Lipofectamine Plus, Life Technologies, Rockville, MD) with pCDNA3 plasmids (10 or 2 µg supercoiled plasmid/dish or well, respectively) containing either no insert or native WT or V230V-WT human opsin cDNAs [48]. Transfected cells were plated on coverslips and processed for rod opsin immunocytochemistry with a COOH-terminal antibody [48].

RESULTS

First and second generation hammerhead ribozyme designs: Efficient hRz cleavage of an mRNA requires accessible regions that permit rapid annealing. A full length human rod opsin mRNA was folded by energy minimization to obtain an estimate of its secondary structural complexity (Figure 2). Few freely accessible regions are apparent. Cleavage sites were sought in single stranded loops capping very stable stems, such that the probability of occurrence of the loop would be high. Similar approaches have been used to identify accessible cleavage sites in large folded mRNAs, which resulted in active hRzs in vivo[28,36,40,55-64]. A hRz GUC‘ cleavage site (785 nt) was identified in an 8 nt single-stranded loop that caps the most stable stem structure in folded mRNA. This GUC triplet codes for Val-230 (V230) and the sequence around this codon does not harbor known opsin adRP mutations. This appeared to be a suitable target for a KD hRz design with broad candidate therapeutic potential.

First generation anti-V230 hRzs were designed around the hRz catalytic consensus core (Figure 1). Relatively long AS flanks (Stem I, 11 nt 5'; Stem III, 12 nt 3') are intended to hybridize to the region around the V230 codon. The total AS flank length (23 nt) has sufficient informational content to specifically recognize rod opsin mRNA among the plethora of mRNAs that are expressed in rod photoreceptors, and the capacity to intrusion anneal into the stable stem structure. BLASTN analysis of the hRz AS sequence against human sequences (with gaps) found only one complete match with human rod opsin mRNA and one nearly complete match with rod opsin pre-mRNA. Partial match clones (up to 16/24 nt) are not specifically expressed in photoreceptors. hRzs targeting V230 GUC‘ in rod opsin mRNA are unlikely to cleave other cellular mRNAs. First generation hRzs did not cleave 1.8 kB WT opsin mRNA by a variety of measures (gel analysis with ethidium, trace-internal, high-specificity end radioactive labeling, or Northern analysis) (data not shown). hRz misfolding can cause catalytic failure [65,66]. hRz RNA structure analysis showed a potential misfolded conformer in first generation hRzs (Figure 3). The correctly folded hRz (I) has a free energy (ΔG) of -1.5 kCal/mol relative to random coil. In the misfolded conformer (II) the 3’ AS flank folds into the Stem II/loop to obviate the active enzyme conformation. II has a ΔG (-3.8 kCal/mol) that is more stable (more negative ΔG) than (I), the active hRz structure, by -2.3 kCal/mol. Equilibrium thermodynamics ($\Delta G=-RT \ln(K_{eq})$) predicts a marked

shift from functional (about 8%) toward misfolded (92%) hRz conformations at 37 °C. This provided a testable hypothesis for first generation failure.

Second generation hRzs were designed to correct misfolding (Rz2A) and stabilize catalytic domain structure (Rz2B) (Figure 1, inset). The AS flanks of the first generation design were maintained. The two nt in the Stem II tetraloop that bond with the 3' AS flank (Figure 1 and Figure 3) were mutated to prevent misfolding and generate a unique XhoI site for the entire hRz plasmid (in pCDNA3). Nucleotides subserving Stem II and its tetraloop are not highly conserved and can be changed without major effects on catalytic activity [1,45,52,67]. In Rz2A the desired hRz structure is most stable with a ΔG equal to -1.5 kCal/mol relative to the random coil. To further stabilize hRz catalytic structure the unique XhoI site was restricted, filled-in and religated to extend Stem II from four to six base pairs in Rz2B (-4.7 kCal/mol). Rz2B is stabilized by -3.2 kCal/mol over Rz2A, which creates a strong thermodynamic bias for hRz folding into an enzymatically-active structure.

Cleavage of expression-competent WT and C187Y mRNAs by second generation V230 ribozymes: Second generation hRzs and opsin mRNA were mixed in a 6:1 molar ratio in 50 mM Tris-HCl (pH 8.0), pre-annealed by brief heating and then slow cooling to 37 °C, before cleavage was initiated by 10 mM $MgCl_2$. "Single-turnover" reaction kinetics prevail ([E] > [S]), where target cleavage is rate limiting (k_{cleave}) over annealing or product (P) dissociation rates. Cleavage of long expression-competent WT or mutant rod opsin mRNAs were analyzed and hRz and Mg^{2+} dependent cleavage were evident (data not shown). Incubations as short as 5-30 min at 37 °C lead to appearance of a clearly detectable 782 nt cleavage product and faint detection of a larger 1056 nt product which overlapped with nonspecific thermochemical degradation products. Increasing reaction time promoted increased conversion of S to cleavage Ps with the maximal extent of product formation at about 20% after 7 h. Most cleavage products are generated in the first 2 h consistent with a burst of cleavage from pre-annealed S molecules [3]. Assuming that all of the [S] (1 μM) is bound to [E] at a 6:1 [E]:[S] molar ratio, we estimate the specific Rz2B k_{cleave} rate to be between 0.001 and 0.005/min. This is several-fold lower than the activity (1/min) of hRzs acting on small targets (ERROR[Basic syntax error] in:<5ERROR[Basic syntax error] in:0 nt) with less secondary structure, but several-fold higher than estimated nonspecific thermochemical rate (about 0.00131/min at 37 °C [3]). The rate estimated is of the same order of magnitude as other hRzs acting against long folded mRNAs [32,68-70].

Can the hRz cleavage products be identified when both the high temperatures needed to promote denaturation and an-

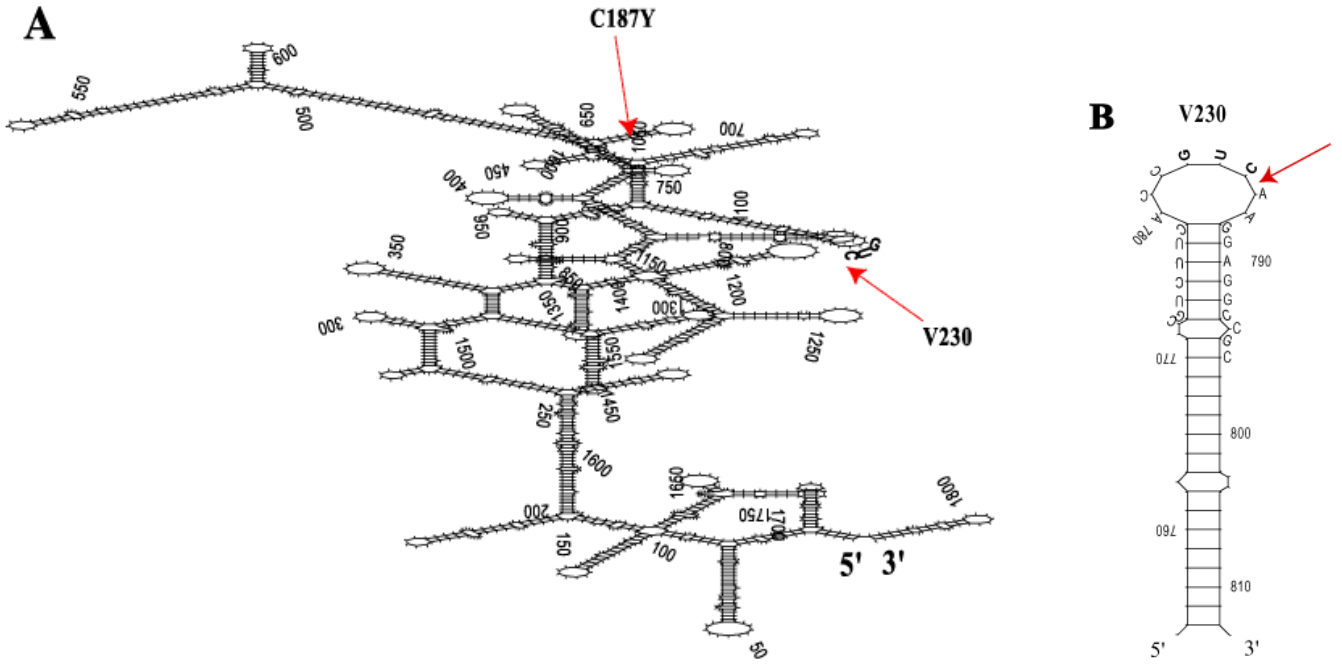

Figure 2. Most stable full length human rod opsin mRNA secondary structure. Full length human rod opsin mRNA from nt 1 (start of transcription) and extending 311 nt beyond the first polyadenylation signal (total 1821 nt length) [46] was subjected to secondary structure folding (RNAFOLD, GCG algorithm) and displayed with SQUIGGLES (GCG). **A**: The most stable secondary structure with the lowest free energy (ΔG=-587.9 kCal/mol) is shown without attempting to rotate regions of overlap. Over 90% of the mRNA is hybridized. Part of the predicted stable stem-loop structure that embraces the V230 codon and the target-annealing region of anti-V230 KD hRzs is annotated by sequence. The cleavage target (GUC') is in bold and the arrow (red) shows the location of the phosphodiester bond broken by anti-V230 hRzs. The adRP C187Y mutation (site not targeted) is shown for reference and is buried in a stem structure. **B**: Magnification of the stem-loop embracing the V230 codon (GUC') shows the sequence that hybridizes to the AS flanks of the first/second generation KD hRzs.

nealing, and the long incubation times are avoided? Conditions were designed to simulate a gene therapy where the hRz RNA would be transcribed from a transgene in photoreceptors (e.g., driven by a rod opsin promoter fragment) at the same time as native opsin mRNA. Linearized opsin and hRz plasmids were mixed to simultaneously transcribe (T7 RNA polymerase) both the S (opsin mRNAs) and E (Rz2A, Rz2B) RNAs in vitro at 37 °C for 1 h. At 37 °C, hRz and S RNAs are transcribed, fold into preferred conformations and participate in cleavage reactions. This avoids RNA aggregates and improperly folded states formed on freezing [52,53], and the high temperatures needed to disperse RNAs and promote annealing that also cause thermochemical RNA breakdown. Figure 4 shows representative results from experiments in which either WT or C187Y opsin mRNA were expressed either alone or simultaneously with one of two second generation hRzs. Rz2A and the more stabilized Rz2B both successfully cleave full length WT and C187Y mRNAs (S) leading to formation of two cleavage Ps of expected size (5': 782 nt and 3': 1056 nt). In fact, both cleavage Ps are identified with low background by SYBR gold probing. The gel is loaded to observe product bands and the S band is broad. Rz2A and Rz2B result in a significant percentage (about 10%) of cleavage products from WT and C187Y mRNAs, so the rate of cleavage was not measurably different. This indicates that the cleavage site in both mRNAs is similarly accessible during transcription and the 1 h incubation at 37 °C. Synthesis of S mRNAs without hRz does not result in cleavage products. The actual cDNA template molar ratio ([S]:[E]) is 6:1 under conditions optimized for transcription initiation of long versus short (e.g., hRzs) templates [50] (T7-MEGAScript kit, Ambion). This is expected to result in S RNA excess and conditions consistent with multiple-turnover kinetics (Michaelis-Menten). Second generation anti-V230 hRzs have catalytic activity under conditions simulating in vivo hRz expression by a rod promoter fragment in a gene therapy.

Cleavage site specificity and the effects of alternatively folded truncated substrate: In vitro cleavage rates of long structured mRNAs (e.g., full length opsin mRNA) are typically one to two orders of magnitude lower than for small "model" S RNAs (about 20 nt) with minimal to no secondary structure (about 1/min for k_{cleave} under [E] excess [32,71]). To further explore second generation anti-V230 hRz cleavage specificity the S template was reduced to a 450 bp opsin cDNA fragment asymmetrically embracing the V230 GUC` site. In vitro transcription yields a 510 nt long RNA S due to added vector sequences. Rz2A and Rz2B attacked the 510 nt S (S) under single turnover conditions (preannealed, [E]:[S]=6:1) initiated by Mg^{2+} (20 mM) at 37 °C or 50 °C for 1 h. Cleavage

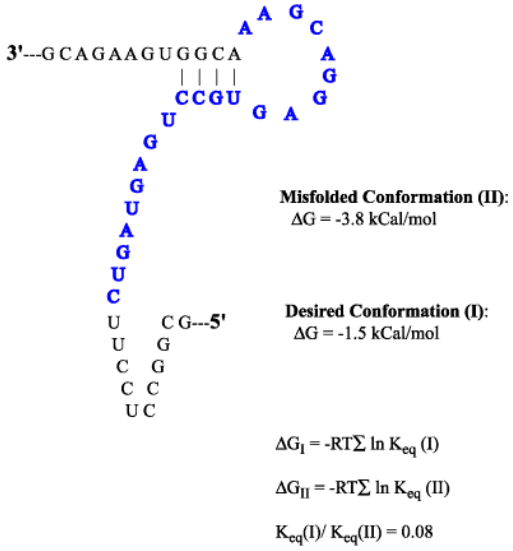

Figure 3. Predicted misfolding of first generation anti-V230 hRz. In the misfolded conformer (II) the 3' AS flank folds anomalously into the StemII/loop domain obviating the formation of an enzymatic structure. The AS flanks are shown in black and the core consensus enzyme in bold blue. The free energies of the misfolded and desired hRz conformations are shown. Thermodynamic equations describing the relationship between ΔG and the equilibrium constant are shown for each conformation. The ratio of the equilibrium constants indicates that the desired enzymatically active conformation is a small fraction of all hRz RNA.

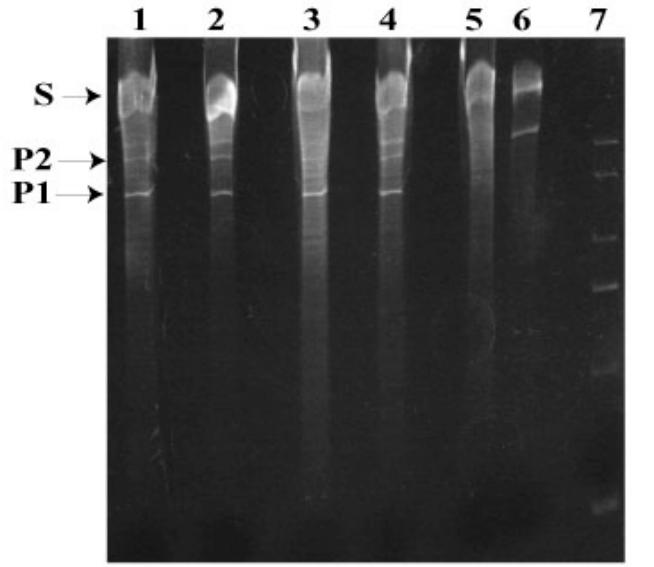

Figure 4. Second generation hRzs Cleave long WT and C187Y opsin mRNAs during co-synthesis/cleavage. Linearized plasmid templates containing opsin or hRz cDNAs downstream of the T7 promoter were mixed in a cDNA template molar ratio of 1:6 ([E]:[S]) and in vitro co-transcription/ cleavage reactions were conducted for 1 h at 37 °C. The reactivities of anti-V230 Rz2A and Rz2B on both WT and C187Y full length mRNAs (S) are shown. Cleavage products (Ps) of expected sizes (P_1=782 nt and P_2=1056 nt) were generated with each hRz reacting with each mRNA target. C187Y and WT mRNAs cut with Rz2A are in lanes 1 and 2, respectively, and the same targets cut with Rz2B are in lanes 3 and 4. C187Y and WT synthesized without hRz plasmid are in lanes 5 and 6, respectively. Lane 7 is an RNA ladder. hRz RNAs (Rz2A 55 nt, Rz2B 61 nt) are not seen in this gel image. The 1.2 kB band seen on all lanes (except 5) is nonspecific and may reflect an incomplete transcript generated by T7 RNA polymerase stalling.

leads to products of expected size of 198 nt (5') and 312 nt (3') (Figure 5A). Surprisingly, little cleavage occurred at 37 °C in comparison to extensive conversion at 50 °C (about 50%).

Reaction temperatures of 50 °C were necessary to generate significant quantities of cleavage products yet the primary sequence of the 510 nt S RNA is more simplified than full length mRNA. While RNA folding algorithms predict that the secondary structure around the V230 stem-loop was stable, experimental results suggest that the shorter S folds into a secondary/tertiary structure(s) at 37 °C with the V230 GUC‘ not as accessible to second generation hRz annealing when compared to the full length opsin mRNA S. Or, the cleavage site in the truncated S is less accessible due to aggregates formed during frozen storage of RNA [52,53]. RNAFOLD analysis of the 510 nt S found a (stable) stem-loop secondary structure around V230 identical to that in the full length mRNA (data not shown). The bands of lower electrophoretic mobility than the truncated S in lanes that contain hRzs may reflect hRz:S complexes that are stable to denaturing gel conditions. Significant amounts of cleavage products of expected size resulted when short S was co-transcribed with second generation hRz at 37 °C (Figure 5B). This suggests that the 510 nt S forms aggregates or tertiary structures during storage that are different from full length mRNA. When AS short S was transcribed with the hRz no cleavage products were found (Figure 5B). Note that the S fluorescence is considerably greater than the hRz band consistent with expectations from the molar template ratios and the transcription conditions that favor a larger transcript. These outcomes provide strong evidence that the 198 nt (5’) and 312 nt (3') cleavage products result from cleavage after the V230 GUC‘ codon.

Formamide promotes cleavage of truncated substrate at 37 °C: To encourage annealing of hRzs to the truncated S at 37 °C we added formamide to the cleavage reactions. Short S and hRz were previously synthesized and stored at -80 °C. Formamide enhances efficiency of hRz cleavage of long native mRNAs [72] because it decreases the melting temperature of hybridized stems in a concentration-dependent manner. Increasing concentrations of deionized formamide (0-20% v/v) at 37 °C promoted Rz2B cleavage of the truncated S into products of anticipated size (molar ratio [E]:[S] 6:1, 1 h reaction) (Figure 6). Both Mg^{2+} and hRz were required for cleavage. At 20% formamide approximately 40% of S is cleaved into products over a 1 h period suggesting a cleavage rate of approximately 0.008/min, a several-fold improvement over estimated rates for the full length S at 37 °C without formamide. Recall the shift of uncleaved S to lower mobility bands in samples with hRz (Figure 5A). The electrophoretic shift may reflect conformational transitions in the S upon hRz annealing [73], or stable adducts of the hRz to cleavage products, since it disappears with increasing formamide. Increased cleavage efficacy may relate to formamide promoting resolution of aggregated S states, more rapid hRz annealing to its target region due to greater accessibility, and more rapid product release and E turnover.

Increased cleavage with greater concentrations of enzyme: Cleavage reactions with Rz2B were conducted with increas-

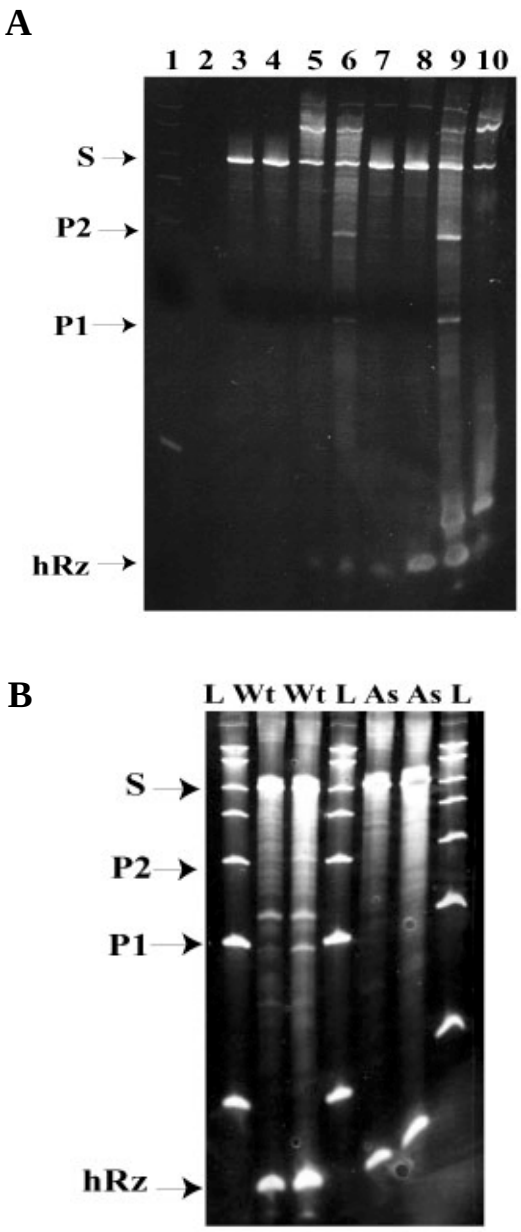

Figure 5. Site specific cleavage of a truncated target affects of alternative substrate structure. **A**: anti-V230 hRzs (Rz2A and Rz2B) were tested against a truncated WT opsin mRNA containing 450 nt of the full length mRNA assymetrically embracing the V230 GUC‘ cleavage site. The truncated S is 510 nt long due to vector sequences read during in vitro transcription. Cleavage at V230 GUC‘ is predicted to yield products P_1 (5’=198 nt) and P_2 (3'=312 nt). Rz2A and Rz2B were reacted with truncated WT S at 37 °C and 50 °C. The E:S ratio was 6:1 (S at 650 nM). Lane 1 is an RNA ladder. Lane 2 is open. Lane 3 and 4 are short WT S at 37 °C and 50 °C, respectively but without hRz and Mg^{2+}. Lanes 5 and 6 are short WT S with Rz2A and Mg^{2+} at 37 °C and 50 °C, respectively. Lanes 7 and 8 are short WT S with Rz2B, 50 °C and 37 °C, respectively but without Mg^{2+}. Lanes 9 and 10 are WT-short with Rz2B and 50 °C and 37 °C, respectively, with Mg^{2+}. **B**: Short WT and short opsin AS constructs were transcribed (in duplicate) with Rz2B ([E]:[S] template ratio 1:6) for 1 h at 37 °C. The label in the header indicates the S used and the lanes with ladders.

ing [E]:[S] ratio while holding truncated [S] (570 nM) and formamide (20% v/v) constant. Increasing [E]:[S] enhances cleavage such that by 50-100:1 ratio about 50% of S is converted to product (Figure 7). This suggests that the second-order annealing reaction is rate limiting to cleavage of the truncated S. Cleavage of 1.8 kB mRNAs without formamide at 37 °C saturated when [E]:[S] ([S]=650 nM) was between 25-50:1 (data not shown). In side-by-side comparisons Stem-II stabilized Rz2B performed slightly better than Rz2A against truncated S (37 °C, 20% v/v formamide).

Rz2B fails to cleave a mutated (GUC‘->GUG) truncated substrate at high molar ratios: A proof of site-specific catalysis by second generation anti-V230 hRzs at the predicted GUC‘ of the V230 codon can be obtained from S mutated at the cleavage site. The V230 codon GUC‘ was silently mutated to GUG, which is not cleaved by the hRz catalytic consensus because the 3’ G nt makes an inactivating hydrogen bond with the catalytic core [74]. Increasing concentrations of Rz2B were reacted with truncated S containing a V230 GUG codon (Figure 8). There is no evidence for cleavage products (198 and 310 nt) (broken arrows) even at [E]:[S] molar ratios of 100:1. We conclude that second generation hRzs cleave precisely at the intended V230 GUC‘ site.

Long expression-competent V230V (GUG) and native WT (V230 GUC) opsin expression plasmids were transfected into HEK293S cells and after two days immunocytochemistry showed that opsin protein was equivalently expressed by both constructs and mostly trafficked to the plasma membrane (data not shown). Since the mRNA for the V230V human rod opsin is not cleaved by second generation hRzs, this construct could be used to reconstitute WT opsin expression in gene therapy protocols employing an anti-V230 KD hRz.

DISCUSSION

KD hRzs cleave long expression-competent human rod opsin mRNAs: These experiments report the first direct proof-of-principle demonstration that small catalytic KD hRzs can be used in vitro to site-specifically cleave functional expression-competent WT and mutant human opsin cRNA targets (1.8 kB) that code for full length protein in live human cells in the context of a gene therapy strategy for adRP. This cRNA target contains an equivalent length 5' untranslated region (92 versus 95 nt) with 21 nt of proximal 5' UT opsin sequence, the complete coding region, and a full 3' untranslated region extending beyond the first polyadenylation signal [46]. This human rod opsin cRNA experimentally simulates the real human mRNA targets that would occur in vivo during ribozyme gene therapy trials for opsin adRP. A major challenge in development of KD hRzs is to identify those few cleavage sites

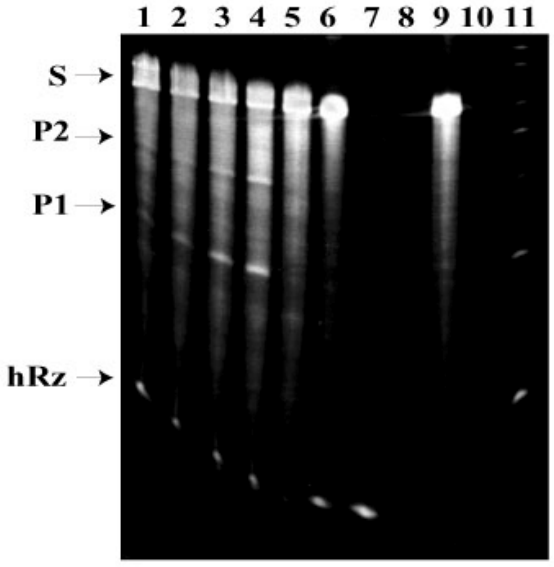

Figure 6. Formamide promotes cleavage of truncated WT substrate at 37 °C. Formamide was added to the cleavage reactions to chaperone annealing and reactivity of second generation anti-V230 hRzs with the WT-truncated S. Formamide enhances hRz cleavage of long native mRNAs [72] by decreasing the melting temperature of hybridized stems in a concentration dependent manner. The panel shows cleavage of the WT truncated S by preannealed Rz2B at 37 °C ([E]:[S] 6:1, S at 650 nM) for 1 h with increasing concentrations of deionized formamide (0-20% v/v), lanes 1 through 4. Lane 5 is the control short S without Rz2B at 0% formamide. Lane 6 is the short S with Rz2B but without Mg^{2+} at 40:1 E:S ratio and without formamide. Lane 7 is Rz2B RNA alone. Lane 8 and 10 are open. Lane 9 is the short S alone. Lane 11 is the RNA ladder.

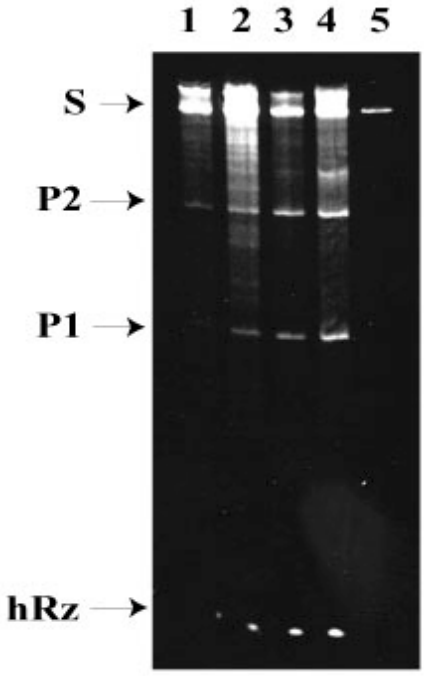

Figure 7. Increased cleavage with greater enzyme concentrations. Cleavage reactions were conducted with increasing [E]:[S] ratio (truncated [S] constant at 650 nM) over a 1 h period at 37 °C in the presence of 20%(v/v) formamide. As the Rz2B concentration increases (lanes 1-4) greater quantities of cleavage products (P1, P2) form such that by 100:1 ratio approximately 40% of S RNA is converted to products. Lane 1 is Rz2B:Short 6:1, Lane 2 is Rz2B:Short 25:1, Lane 3 is Rz2B:Short 50:1, Lane 4 is Rz2B:Short 100:1. Lane 5 has Short S without Rz2B in 20% formamide. Note the doublet S bands that appear in the presence of hRz.

in the mRNA that are accessible to rapid hRz annealing and not impeded by secondary or tertiary structure [27-40]. hRzs recognize sequence triplets of the form NUH‘ (N=G,C,U,A; H=C,U,A) where the ‘ marks the scission phosphodiester bond. The first cleavage site targeted was a GUC‘ motif (Valine-230 codon) that resides in a predicted single-stranded loop at the end of a stable stem. We reasoned that this loop would offer a sterically accessible docking site to seed hRz AS annealing. We empirically demonstrate that the V230 GUC‘ site is accessible to hRz cleavage in long expression-competent WT and mutant C187Y mRNAs, both during and after transcription. The C187Y mutation causes opsin misfolding and promotes a severe, early onset, and rapidly progressive form of adRP [41,75]. The V230 GUC‘ cleavage motif is not affected by any known adRP rod opsin mutations such that the KD hRzs developed in this work should be equivalently effective to cleave all currently known adRP-causing opsin mRNAs.

Second generation KD hRzs cleaved functional human opsin mRNAs to yield products of expected size with up to 20% target conversion with the hRz in excess. Products of expected sizes also occurred with truncated WT cRNA. This suggested site-specific cleavage after the V230 GUC‘ codon, which was proven when second generation hRzs failed to cleave a truncated target containing a noncleavable V230 GUG codon, or an AS RNA derived from the same fragment of WT cDNA. V230 GUC‘ is accessible in full length opsin mRNA at 37 °C in vitro during transcription and cRNA accumulation, conditions that simulate transcription and long-lived cytoplasmic accumulation in vivo [76,77].

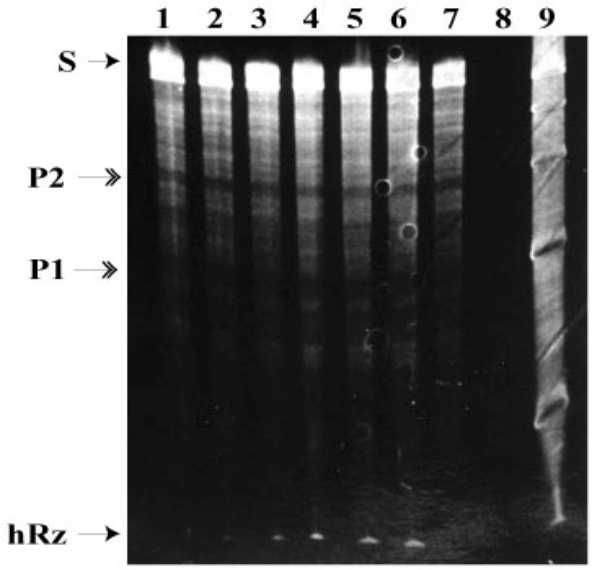

Figure 8. Rz2B fails to cleave a tempered (GUC‘->GUG, V230V) substrate. The V230 codon GUC‘ was silently mutagenized to GUG (V230V), which continues to code for valine but GUG is not cleaved by a hRz. The change was engineered into the truncated V230V opsin S mRNA (510 nt) and cleavage reactions were conducted at a [S] concentration of 556 nM in 20% v/v formamide. Increasing the molar ratio of Rz2B:[V230V GUG S] does not promote S cleavage over 1 h at 37 °C. Lanes 1-6 show [E]:[S] ratios at 1:1, 6:1, 10:1, 25:1, 50:1, and 100:1. The [E]:[S] ratio is shown in the header. Lane 7 is a cleavage reaction without Rz2B, and Lane 9 is an RNA ladder. The position of the broken arrows indicates the expected location of the products (198 nt, 310 nt) if Rz2B cleavage had occurred at the V230 site. The background degradation represents nonspecific thermochemical cleavage or incomplete transcription products. If cleavage products had occurred they would have appeared in the low background regions found in each lane and would have been easy to recognize, especially since the same reaction conditions support approximately 50% cleavage of WT truncated S.

Alternative structures of the target RNA and ribozyme impact cleavage efficacy

Substrate Structure: At 37 °C the V230 GUC‘ cleavage site is less accessible in the frozen-stored truncated target (510 nt) versus the long expression-competent mRNA (1838 nt). The truncated substrate is cleaved more efficiently at 50 °C than at 37 °C. Higher temperatures or formamide (37 °C) are necessary to expose the V230 GUC‘ cleavage motif for reaction with second generation hRzs in frozen-stored truncated WT target. Formamide decreases the melting temperature of RNA secondary/tertiary structures in a concentration-dependent manner and stimulates hRz reactivity against native mRNAs [72]. This mimics the chaperoning effects of ribonucleoproteins on ribozyme activity [78]. Clear differences in accessibility to hRz cleavage at the V230 cleavage site occur in experiments with frozen-stored full length versus truncated targets. However, the WT truncated target cleaves the V230 site at 37 °C in co-transcription/cleavage reactions. This suggests that decreased accessibility of V230 GUC‘ in the frozen-stored versus freshly synthesized truncated WT target is caused by frozen storage. Other studies suggest that frozen storage of RNA solutions can lead to RNA aggregates that impair ribozyme cleavage reactions [51,52]. Even gel purification can result in functional changes in RNA structure [53]. We hypothesize that alternative RNA structure(s) around the V230 cleavage site in truncated versus long functional WT mRNA explain the differential accessibility to hRz cleavage.

Conformational complexity and dynamics of native-length mRNAs are vast. Predicted secondary structures of full length mRNA (Figure 1) are a snapshot of the conformational landscape available to any mRNA [79]. Regional accessibility of mRNA fluctuates dynamically in vitro and in vivo and few environments, on average, will have sufficient lifetime to allow significant hRz cleavage to impact upon gene expression. Moreover, mRNA has extensive interactions with proteins in cells that shape local structure and dynamics [80]. Extensive evidence from AS and Rz studies indicates that few potential target sites are sterically or energetically accessible to the rate limiting annealing step in native mRNAs [27-40]. We expect that most of the 236 potential NUH‘ cleavage sites in full length human rod opsin mRNA will not be sufficiently accessible to support robust KD hRz cleavage in vitro or in vivo. Processing streams, cellular compartments, and natural mRNA target lifetimes add constraints that further limit Rz efficacy in cells. We employ a Rational hRz design strategy that starts with predictors of conformational accessibility. hRzs targeting candidate sites are tested empirically both in vitro, as done here, and in human cells expressing the human target mRNA and protein, where high throughput evaluation of candidates is

feasible. Energy-based accessibility predictors, combined with empirical testing in vitro, have lead to hRz or AS designs that impacted target gene expression in vivo [28,36,55-64,79].

Enzyme structure: First generation anti-V230 hRzs failed to cleave opsin mRNA. Correction of a putative misfolded conformation, by mutations at nonconserved nucleotides in the hRz core, lead to second generation hRzs that successfully cleaved both WT and C187Y opsin mRNAs at the V230 GUC‘ codon at 37 °C. This proved that this hRz must fold correctly for catalysis [65]. Limited extension of Stem II biases the energetics of hRz folding to insure structural stability supportive of catalysis. The conditions of second generation hRz cleavage in this study demonstrated significant conversion of S to products (Ps) but not beyond 50% under conditions of up to 100-fold molar E excess for the truncated S and not beyond 20% for full length S, regardless of E or S excess. Lack of complete cleavage reflects S and E features. The accessibility around V230 GUC‘ plays a role in how well the site can be targeted. The single-stranded loop that contains the targeted GUC‘ cleavage moiety is only 8 nt long (Figure 1B). This leaves only 7 nt for the proximate AS flanks of second generation anti-V230 hRzs to form an initial hybridization seeding complex with the mRNA. The remainder of each AS flank would encounter asymmetric energy barriers to intrusion anneal into hybridized stem structure [remainders: 5’ flank (Stem I), 9 nt; 3' flank (Stem III), 7 nt] (Figure 1). The AS flank lengths (12 nt and 11 nt) were engineered, in part, to drive hybridization into the stable stem structure. However, this occurs with a price. Once fully and properly annealed the second generation hRzs cleave opsin mRNA, but product dissociation rates at 37 °C appear slow and these likely limit robust turnover. The incomplete cleavage of mRNA in vitro is likely due to limited accessibility of the entire docking domain to rapid hRz:mRNA complex formation, energetic barriers to complete annealing, and limited product dissociation rates. These constraints also play a major role in the often sub quantitative cleavage efficiency of full length mRNA targets both in vitro and in vivo and the typical requirement of high [E]:[S] ratios to drive cleavage to its maximal extent. The hRz annealing reaction should achieve a rapid equilibrium prior to chemical cleavage (maximum about 1/min) to improve catalytic turnover (S>E) and insure site-specific cleavage [2,71]. Next generation KD hRz designs targeting V230 GUC‘ have shortened AS flanks to both decrease the energetic barriers to full annealing and improve product dissociation rates at 37 °C [71].

Major advantages and disadvantages of a KD ribozyme strategy: The KD strategy is designed to cleave both mutant and WT mRNAs. KD takes the approach used in anti-viral Rz strategies, that the most efficacious Rz would target a cleavage site residing in a sterically accessible unhybridized single-stranded loop or in a region of low hybridization energy [27-40,55-64]. The challenge is to identify the best cleavage site that is present in both mutant and WT mRNAs. Highly accessible ribozyme cleavage sites occur with low probability in mRNAs of average size [30-37]. A major advantage of KD is that a single efficacious Rz, targeting a single highly accessible cleavage site present in both the WT and mutant mRNAs, could be used to treat all human autosomal dominant mutations in a given arbitrary disease gene. This is not possible in Mutation-Directed strategies (MSpe, MSel) because the mutation independently obligates the region of each mutant mRNA targeted. The KD strategy could lead to rapid identification of candidate Rz therapeutics for a wide range of patients at considerably lower cost for development in comparison to the mutation directed strategies.

A potential downside of KD is the lack of preferred cleavage of mutant versus WT mRNA. WT and mutant proteins are suppressed. The abundance of WT rhodopsin in rod photoreceptors and the established ranges of WT rod opsin suppression tolerated in human (≥50%), mouse (≥50%), and rat (≥75%) rod photoreceptors were presented. Cells affected by an autosomal dominant degeneration are likely to contain approximately 50% WT protein and 50% mutant. A successful KD hRz will suppress WT and mutant protein further. The regular KD strategy may be sufficient for a gene expressed to such great abundance as opsin, provided that cell survival does not depend upon an excess of WT over mutant protein. The suppression of deleterious effects of mutant protein expression is likely to offset the loss of WT protein [81]. However, a regular KD approach may not be protective and could be deleterious for an autosomal dominant disease gene expressed at much lower abundance, or when cell survival requires WT protein in excess of mutant [15]. A solution to this problem is combined gene therapy. A KD ribozyme is expressed in combination with a WT reconstitution gene, which is an allele engineered to transcribe a tempered mRNA that cannot be cleaved by the KD ribozyme, yet reconstitutes WT opsin protein expression. This approach was first reported for dominant hereditary diseases [23] and autosomal dominant retinal degenerations [24,25], and more recently for other dominant somatic diseases [26]. The “full length” opsin cDNA used here expresses abundant mRNA and protein from the CMV promoter in human cells [48]. We constructed a WT reconstitution cDNA (V230V) that is transcribed into a tempered mRNA that is not cleaved by anti-V230 hRzs. We report here, for the first time, that a reconstituting WT opsin cDNA (V230V) expresses an mRNA in human cells that translates full length WT opsin protein in vivo which was detected by a monoclonal antibody recognizing a COOH-terminal epitope. This allelic variant WT cDNA could be used to reconstitute WT opsin protein in a combined KD gene therapy with an anti-V230 GUC` hRz.

After our work was submitted for publication we became aware of another study [82] where four sites in the coding region of rod opsin mRNA were targeted with hRzs. One of those sites was the V230 GUC‘ cleavage site. Critically, in this study the V230 hRz was not tested in isolation. Rather, the V230 GUC‘ site was targeted, in part, by a multimeric hRz with four hRzs in tandem linkage each targeting serial sites in the opsin mRNA (Val61 GUC‘, Leu84 CUC‘, Leu95 CUC‘, Val230 GUC‘). We were unable to determine, from the data presented (Figure 4F in [82]), how well the anti-V230 component of this ribozyme is functioning in vitro because of

lack of independence of each hRz and a multiplicity of potential cleavage products that were not labeled. We folded the tandem hRz (RzMM [82]) sequence with MFOLD (37 °C) and found in all outputs (6/6) that the V230 hRz component was at least partially misfolded, with either one or both AS flanks trapped and the core enzyme sequences at least partially hybridized, and therefore likely inactive.

In summary, we present evidence that the V230 GUC‘ site is accessible in a folded full length opsin mRNA and can be cleaved by independently functional anti-V230 hRzs at rates comparable to hRzs targeting sites in native length mRNAs. These hRzs may be candidate gene therapy agents, if they suppress mutant opsin protein expression in human cells, as in vitro cleavage may not obligate equivalent levels of intracellular performance [83]. Experiments are in progress to identify regions of greater accessibility in full length human rod opsin mRNA and to screen these and other hRzs in different expression cassettes in high throughput cellular expression systems.

ACKNOWLEDGEMENTS

The project was conceived during a Career Development Award (JMS) from the Foundation Fighting Blindness (Harry J. Hocks Memorial funds). Work was supported by the Department of Ophthalmology through the Research Foundation of the State of New York and a Challenge Grant from Research to Prevent Blindness (Department of Ophthalmology, SUNY Upstate Medical University). We acknowledge the participation of Rachel C. Jansen, M.S. and Eileen Luque, M.D., Ph.D. in preliminary experiments leading to this study on second-generation ribozymes. We acknowledge the construction of the C187Y human opsin cDNA by Steven Jansen (SUNY Summer Undergraduate Research Fellowship program). We appreciate the gift of normal human rod opsin cDNA from Jeremy Nathans, M.D., Ph.D. (Johns Hopkins) and the gift of HEK293S cells from Bruce Stillman, Ph.D. (Cold Spring Harbor). We appreciate discussions on the application of ribozymes with Edward Shillitoe, Ph.D. (Department of Microbiology, SUNY Upstate Medical University).

REFERENCES

1. Haseloff J, Gerlach WL. Simple RNA enzymes with new and highly specific endoribonuclease activities. Nature 1988; 334:585-91.
2. Herschlag D. Implications of ribozyme kinetics for targeting the cleavage of specific RNA molecules in vivo: more isn’t always better. Proc Natl Acad Sci U S A 1991; 88:6921-5.
3. Hertel KJ, Peracchi A, Uhlenbeck OC, Herschlag D. Use of intrinsic binding energy for catalysis by an RNA enzyme. Proc Natl Acad Sci U S A 1997; 94:8497-502.
4. Drenser KA, Timmers AM, Hauswirth WW, Lewin AS. Ribozyme-targeted destruction of RNA associated with autosomal-dominant retinitis pigmentosa. Invest Ophthalmol Vis Sci 1998; 39:681-9.
5. Lewin AS, Drenser KA, Hauswirth WW, Nishikawa S, Yasamura D, Flannery JG, LaVail MM. Ribozyme rescue of photoreceptor cells in transgenic rat model of autosomal dominant retinitis pigmentosa. Nat Med 1998; 4:967-71.
6. Shimayama T, Nishikawa S, Taira K. Generality of the NUX rule: kinetic analysis of the results of systematic mutations in the trinucleotide at the cleavage site of hammerhead ribozymes. Biochemistry 1995; 34:3649-54.
7. Zoumadakis M, Tabler M. Comparative analysis of cleavage rates after systematic permutation of the NUX consensus target motif for hammerhead ribozymes. Nucleic Acids Res 1995; 23:1192-6.
8. Koizumi M, Hayase Y, Iwai S, Kamiya H, Inoue H, Ohtsuka E. Design of RNA enzymes distinguishing a single base mutation in RNA. Nucleic Acids Res 1989; 17:7059-71.
9. Werner M, Uhlenbeck OC. The effect of base mismatches in the substrate recognition helices of hammerhead ribozymes on binding and catalysis. Nucleic Acids Res 1995; 23:2092-6.
10. Gal A, Apfelstedt-Sylla E, Janecke AR, Zrenner E. Rhodopsin mutations in inherited retinal dystrophies and dysfunctions. Prog Retin Eye Res 1997; 16:51-79.
11. Sandberg MA, Weigel-DiFranco C, Dryja TP, Berson EL. Clinical expression correlates with location of rhodopsin mutation in dominant retinitis pigmentosa. Invest Ophthalmol Vis Sci 1995; 36:1934-42.
12. Sung CH, Schneider BG, Agarwal N, Papermaster DS, Nathans J. Functional heterogeneity of mutant rhodopsins responsible for autosomal dominant retinitis pigmentosa. Proc Natl Acad Sci U S A 1991; 88:8840-4.
13. Fain GL, Lisman JE. Photoreceptor degeneration in vitamin A deprivation and retinitis pigmentosa: the equivalent light hypothesis. Exp Eye Res 1993; 57:335-40.
14. Colley NJ, Cassill JA, Baker EK, Zuker CS. Defective intracellular transport is the molecular basis of rhodopsin-dependent dominant retinal degeneration. Proc Natl Acad Sci U S A 1995; 92:3070-4.
15. Frederick JM, Krasnoperova NV, Hoffmann K, Church-Kopish J, Ruther K, Howes K, Lem J, Baehr W. Mutant rhodopsin transgene expression on a null background. Invest Ophthalmol Vis Sci 2001; 42:826-33.
16. Chang GQ, Hao Y, Wong F. Apoptosis: final common pathway of photoreceptor death in rd, rds, and rhodopsin mutant mice. Neuron 1993; 11:595-605.
17. Portera-Cailliau C, Sung CH, Nathans J, Adler R. Apoptotic photoreceptor cell death in mouse models of retinitis pigmentosa. Proc Natl Acad Sci U S A 1994; 91:974-8.
18. Kraft TW, Schneeweis DM, Schnapf JL. Visual transduction in human rod photoreceptors. J Physiol 1993; 464:747-65.
19. Rosenfeld PJ, Cowley GS, McGee TL, Sandberg MA, Berson EL, Dryja TP. A null mutation in the rhodopsin gene causes rod photoreceptor dysfunction and autosomal recessive retinitis pigmentosa. Nat Genet 1992; 1:209-13.
20. Rosenfeld PJ, Hahn LB, Sandberg MA, Dryja TP, Berson EL. Low incidence of retinitis pigmentosa among heterozygous carriers of a specific rhodopsin splice mutation. Invest Ophthal Vis Sci 1995; 36:2186-92.
21. Humphries MM, Rancourt D, Farrar GJ, Kenna P, Hazel M, Bush RA, Sieving PA, Sheils DM, McNally N, Creighton P, Erven A, Boros A, Gulya K, Capecchi MR, Humphries P. Retinopathy induced in mice by targeted disruption of the rhodopsin gene. Nat Genet 1997; 15:216-9.
22. Penn JS, Williams TP. Photostasis: regulation of daily photon-catch by rat retinas in response to various cyclic illuminances. Exp Eye Res 1986; 43:915-28.
23. Montgomery RA, Dietz HC. Inhibition of fibrillin 1 expression using U1 snRNA as a vehicle for the presentation of antisense targeting sequence. Hum Mol Genet 1997; 6:519-25.
24. Millington-Ward S, O’Neill B, Tuohy G, Al-Jandal N, Kiang AS,

Kenna PF, Palfi A, Hayden P, Mansergh F, Kennan A, Humphries P, Farrar GJ. Strategems in vitro for gene therapies directed to dominant mutations. Hum Mol Genet 1997; 6:1415-26.
25. Sullivan JM, Pietras KM, Shin BJ. Design and testing of hammerhead ribozymes to cleave full-length opsin mRNA. Invest Ophthalmol Vis Sci 1998; 39:S722.
26. Ozaki I, Zern MA, Liu S, Wei DL, Pomerantz RJ, Duan L. Ribozyme-mediated specific gene replacement of the alpha 1-antitrypsin gene in human hepatoma cells. J Hepatol 1999; 31:53-60.
27. Taylor NR, Rossi JJ. Ribozyme-mediated cleavage of an HIV-1 gag RNA: the effects of nontargeted sequences and secondary structure on ribozyme cleavage activity. Antisense Res Dev 1991; 1:173-86.
28. Xing, Z, Whitton JL. Ribozymes which cleave arenavirus RNAs: identification of susceptible target sites and inhibition by target site secondary structure. J Virol 1992; 66:1361-9.
29. Scarabino D, Tocchini-Valentini GP. Influence of substrate structure on cleavage by hammerhead ribozyme. FEBS Lett 1996; 383:185-90.
30. Ho SP, Britton DH, Stone BA, Behrens DL, Leffet LM, Hobbs FW, Miller JA, Trainor GL. Potent antisense oligonucleotides to the human multidrug resistance-1 mRNA are rationally selected by mapping RNA-accessible sites with oligonucleotide libraries. Nucleic Acids Res 1996; 24:1901-7.
31. Birikh KR, Berlin YA, Soreq H, Eckstein F. Probing accessible sites for ribozymes on human acetylcholinesterase RNA. RNA 1997; 3:429-37.
32. Campbell TB, McDonald CK, Hagen M. The effect of structure in a long target RNA on ribozyme cleavage efficiency. Nucleic Acids Res 1997; 25:4985-93.
33. Milner N, Mir KU, Southern EM. Selecting effective antisense reagents on combinatorial oligonucleotide arrays. Nat Biotechnol 1997; 15:537-41.
34. Ho SP, Bao Y, Lesher T, Malhotra R, Ma LY, Fluharty SJ, Sakai RR. Mapping of RNA accessible sites for antisense experiments with oligonucleotide libraries. Nat Biotechnol 1998; 16:59-63.
35. Yu Q, Pecchia DB, Kingsley SL, Heckman JE, Burke JM. Cleavage of highly structured viral RNA molecules by combinatorial libraries of hairpin ribozymes. The most effective ribozymes are not predicted by substrate selection rules. J Biol Chem 1998; 273:23524-33.
36. Scherr M, Rossi JJ. Rapid determination and quantitation of the accessibility to native RNAs by antisense oligodeoxynucleotides in murine cell extracts. Nucleic Acids Res 1998; 26:5079-85.
37. zu Putlitz J, Yu Q, Burke JM, Wands JR. Combinatorial screening and intracellular antiviral activity of hairpin ribozymes directed against hepatitis B virus. J Virol 1999; 73:5381-7.
38. Vickers TA, Wyatt JR, Freier SM. Effects of RNA secondary structure on cellular antisense activity. Nucleic Acids Res 2000; 28:1340-7.
39. Rittner K, Burmester C, Sczakiel G. In vitro selection of fast-hybridizing and effective antisense RNAs directed against the human immunodeficiency virus type 1. Nucleic Acids Res 1993; 21:1381-7.
40. Patzel V, Sczakiel G. Theoretical design of antisense RNA structures substantially improves annealing kinetics and efficacy in human cells. Nat Biotechnol 1998; 16:64-8.
41. Richards JE, Scott KM, Sieving PA. Disruption of conserved rhodopsin disulfide bond by Cys187Tyr mutation causes early and severe autosomal dominant retinitis pigmentosa. Ophthalmology 1995; 102:669-77.
42. Devereux J, Haeberli P, Smithies O. A comprehensive set of sequence analysis programs for the VAX. Nucleic Acids Res 1984; 12:387-95.
43. Zuker M, Stiegler P. Optimal computer folding of large RNA sequences using thermodynamics and auxiliary information. Nucleic Acids Res 1981; 9:133-48.
44. Jaeger JA, Turner DH, Zuker M. Improved predictions of secondary structures for RNA. Proc Natl Acad Sci U S A 1989; 86:7706-10.
45. Ruffner DE, Stormo GD, Uhlenbeck OC. Sequence requirements of the hammerhead RNA self-cleavage reaction. Biochemistry 1990; 29:10695-702.
46. Nathans J, Hogness DS. Isolation and nucleotide sequence of the gene encoding human rhodopsin. Proc Natl Acad Sci U S A 1984; 81:3851-5.
47. Deng WP, Nickoloff JA. Site-directed mutagenesis of virtually any plasmid by eliminating a unique site. Anal Biochem 1992; 200:81-8.
48. Sullivan JM, Satchwell MF. Development of stable cell lines expressing high levels of point mutants of human opsin for biochemical and biophysical studies. Methods Enzymol 2000; 315:30-58.
49. Homann M, Tabler M, Tzortzakaki S, Sczakiel G. Extension of helix II of an HIV-1-directed hammerhead ribozyme with long antisense flanks does not alter kinetic parameters in vitro but causes loss of the inhibitory potential in living cells. Nucleic Acids Res 1994; 22:3951-7.
50. Pokrovskaya ID, Gurevich VV. In vitro transcription: preparative RNA yields in analytical scale reactions. Anal Biochem 1994; 220:420-3.
51. Fedor MJ, Uhlenbeck OC. Substrate sequence effects on “hammerhead” RNA catalytic efficiency. Proc Natl Acad Sci U S A 1990; 87:1668-72.
52. Fedor MJ, Uhlenbeck OC. Kinetics of intermolecular cleavage by hammerhead ribozymes. Biochemistry 1992; 31:12042-54.
53. Walstrum SA, Uhlenbeck OC. The self-splicing RNA of Tetrahymena is trapped in a less active conformation by gel purification. Biochemistry 1990; 29:10573-6.
54. Stillman BW, Gluzman Y. Replication and supercoiling of simian virus 40 DNA in cell extracts from human cells. Mol Cell Biol 1985; 5:2051-60.
55. Stull RA, Taylor LA, Szoka FC Jr. Predicting antisense oligonucleotide inhibitory efficacy: a computational approach using histograms and thermodynamic indices. Nucleic Acids Res 1992; 20:3501-8.
56. Sczakiel G, Homann M, Rittner K. Computer-aided search for effective antisense RNA target sequences of the human immunodeficiency virus type 1. Antisense Res Dev 1993; 3:45-52.
57. Sczakiel G, Tabler M. Computer-aided calculation of the local folding potential of target RNA and its use for ribozyme design. In: Turner PC, editor. Methods in molecular biology. Ribozyme protocols, vol 74. Totowa (NJ): Humana Press; 1997. p 11-15.
58. James W, Cowe E. Computational approaches to the identification of ribozyme target sites. In: Turner PC, editor. Methods in molecular biology. Ribozyme protocols, vol 74. Totowa (NJ): Humana Press; 1997. p 17-26.
59. Matveeva O, Felden B, Audlin S, Gesteland RF, Atkins JF. A rapid in vitro method for obtaining RNA accessibility patterns for complementary DNA probes: correlation with an intracellular pattern and known RNA structures. Nucleic Acids Res 1997; 25:5010-6.
60. Patzel V, Steidl U, Kronenwett R, Haas R, Sczakiel G. A theoretical approach to select effective antisense oligodeoxyribonucleotides at high statistical probability. Nucleic

Acids Res 1999; 27:4328-34.
61. Scherr M, Rossi JJ, Sczakiel G, Patzel V. RNA accessibility prediction: a theoretical approach is consistent with experimental studies in cell extracts. Nucleic Acids Res 2000; 28:2455-61.
62. Scherr M, Reed M, Huang CF, Riggs AD, Rossi JJ. Oligonucleotide scanning of native mRNAs in extracts predicts intracellular ribozyme efficiency: ribozyme-mediated reduction of the murine DNA methyltransferase. Mol Ther 2000; 2:26-38.
63. Amarzguioui M, Brede G, Babaie E, Grotli M, Sproat B, Prydz H. Secondary structure prediction and in vitro accessibility of mRNA as tools in the selection of target sites for ribozymes. Nucleic Acids Res 2000; 28:4113-24.
64. Ding Y, Lawrence CE. Statistical prediction of single-stranded regions in RNA secondary structure and application to predicting effective antisense targets sites and beyond. Nucleic Acids Res 2001; 29:1034-46.
65. Christoffersen RE, McSwiggen JM, Konings D. Application of computational technologies to ribozyme biotechnology products. J Mol Struct 1994; 311:272-84.
66. Palfner K, Kneba M, Hiddemann W, Bertram J. Improvement of hammerhead ribozymes cleaving mdr-1 mRNA. Biol Chem Hoppe Seyler 1995; 376:289-95.
67. Long DM, Uhlenbeck OC. Kinetic characterization of intramolecular and intermolecular hammerhead RNAs with stem II deletions. Proc Natl Acad Sci U S A 1994; 91:6977-81.
68. Heidenreich O, Eckstein F. Hammerhead ribozyme-mediated cleavage of the long terminal repeat RNA of human immunodeficiency virus type I. J Biol Chem 1992; 267:1904-9.
69. Ellis J, Rogers J. Design and specificity of hammerhead ribozymes against calretinin mRNA. Nucleic Acids Res 1993; 21:5171-8.
70. Hendrix C, Anne J, Joris B, Van Aerschot A, Herdewijn P. Selection of hammerhead ribozymes for optimum cleavage of interleukin 6 mRNA. Biochem J 1996; 314:655-61.
71. Stage-Zimmermann TK, Uhlenbeck OC. Hammerhead ribozyme kinetics. RNA 1998; 4:875-89.
72. Kisich KO, Freedland SJ, Erickson KL. Factors altering ribozyme-mediated cleavage of tumor necrosis factor-alpha mRNA in vitro. Biochem Biophys Res Commun 1997; 236:205-11.
73. Woisard A, Fourrey JL, Favre A. Multiple folded conformations of a hammerhead ribozyme domain under cleavage conditions. J Mol Biol 1994; 239:366-70.
74. Simorre JP, Legault P, Baidya N, Uhlenbeck OC, Maloney L, Wincott F, Usman N, Beigelman L, Pardi A. Structural variation induced by different nucleotides at the cleavage site of the hammerhead ribozyme. Biochemistry 1998; 37:4034-44.
75. Karnik SS, Khorana HG. Assembly of functional rhodopsin requires a disulfide bond between cysteine residues 110 and 187. J Biol Chem 1990; 265:17520-4.
76. Korenbrot JI, Fernald RD. Circadian rhythm and light regulate opsin mRNA in rod photoreceptors. Nature 1989; 337:454-7.
77. McGinnis JF, Whelan JP, Donoso LA. Transient, cyclic changes in mouse visual cell gene products during light-dark cycle. J Neurosci Res 1992; 31:584-90.
78. Herschlag D, Khosla M, Tsuchihashi Z, Karpel RL. An RNA chaperone activity of non-specific RNA binding proteins in hammerhead ribozyme catalysis. EMBO J 1994; 13:2913-24.
79. Mathews DH, Sabina J, Zuker M, Turner DH. Expanded sequence dependence of thermodynamic parameters improves prediction of RNA secondary structure. J Mol Biol 1999; 288:911-40.
80. Herschlag D. RNA chaperones and the RNA folding problem. J Biol Chem 1995; 270:20871-4.
81. McInnes RR, Bascom RA. Retinal genetics: a nullifying effect for rhodopsin. Nat Genet 1992; 1:155-7.
82. O'Neill B, Millington-Ward S, O'Reilly M, Tuoby G, Kiang AS, Kenna PF, Humphries P, Farrar GJ. Ribozyme-based therapeutic approaches for autosomal dominant retinitis pigmentosa. Invest Ophthalmol Vis Sci 2000; 41:2863-9.
83. Beck J, Nassal M. Efficient hammerhead ribozyme-mediated cleavage of the structured hepatitis B virus encapsidation signal in vitro and in cell extracts, but not in intact cells. Nucleic Acids Res 1995; 23:4954-62.

The print version of this article was created on 10 April 2002. This reflects all typographical corrections and errata to the article through that date. Details of any changes may be found in the online version of the article.